Electronic Supplementary Material (ESI) for Journal of Materials Chemistry B.

Investigation on the elasticity of functional gold nanoparticles using single-molecule force spectroscopy

Li Sun[1,2], René Riedel[3], Stefan G. Stanciu[4], Fang Yang[2,3,5*], Norbert Hampp[3], Li Xu[1*], Aiguo Wu[2,3,5*]

[1] College of Science, Nanjing Forestry University, Nanjing, Jiangsu, PR China
[2] CAS Key Laboratory of Magnetic Materials and Devices & Key Laboratory of Additive Manufacturing Materials of Zhejiang Province & Division of Functional Materials and Nanodevices, Ningbo Institute of Materials Technology and Engineering, Chinese Academy of Sciences, Ningbo, PR China;
[3] Fachbereich Chemie, Philipps Universität Marburg, Marburg, Germany
[4] Center for Microscopy-Microanalysis and Information Processing, University Politehnica Bucharest, Bucharest, Romania
[5] Cixi Institute of BioMedical Engineering, Ningbo Institute of Materials Technology and Engineering, Chinese Academy of Sciences, Ningbo, PR China

*corresponding author: yangf@nimte.ac.cn; xuliqby@njfu.edu.cn; aiguo@nimte.ac.cn

Supporting information

I) Basic principle of AFM

Single Molecule Force Spectroscopy (SMFS) studies can be mainly performed via three avenues: optical tweezers, magnetic tweezers and atomic force microscopy[1], the latter being by far the most popular choice. SMFS systems built on top an underlying Atomic Force Microscope (AFM), benefit of intrinsic registration of force data sets and topography information. The working principles of Atomic Force Microscopy rely on a sharp probe that is fixed at the free end of a cantilever and scanned over the sample surface[2] (see Figure S1). The cantilever bends as it travels along the sample surface according to the van der Waals interactions that occur between the tip and the sample. A laser beam is focused onto the backside of the cantilever and reflected onto a photodiode. Cantilever deflection results in a change of the laser beam's spot position on the photodiode. In contact mode, the tip scans the sample while being in close contact with its surface, the force between the two being repulsive. This force is kept constant by readjusting the cantilevers height at each point, with a piezoelectric positioning element. For soft samples, e.g. biological items, the typical force levels in contact mode can influence the sample topography. To avoid this, the tapping mode of AFM exploits the fact that the tip can be brought to oscillation near its resonance frequency and scanned across the sample surface at an offset distance so that nearfield interaction occurs only shortly during an oscillation circle (see Figure S2). As the oscillating cantilever intermittently contacts the surface, its oscillation amplitude depends on the height of the surface features that are encountered. When high features are met, the amplitude of oscillation decreases as the cantilever has less room to oscillate and conversely, when the tip passes over a depression, the amplitude increases. In this work-mode interaction forces are minimized while the high resolution capabilities are preserved. From these modifications, the topography of the sample can be calculated and represented with very high precision. Besides providing information of the sample surface topography, tip scanning can also be used to map with xy nanoscale precision electrical, magnetical, optical and mechanical properties of a sample[3]. The latter have been proven to represent a factor that has deep implications for the nanoparticles-cell interaction. To determine the mechanical properties of a sample with AFM based setups, the probe is positioned right above the sample and then indented until a certain force is reached (Scheme I in manuscript). Subsequently, the probe is retracted to the initial position. The force can be derived from the cantilever deflection by calibration and is plotted versus the vertical position of the cantilever, resulting in a so-called force-distance curve from which all mechanical properties can be calculated[4]. The cantilever used to measure force-distance curves should be chosen according to the expected sample modulus[5]. Softer probes should be used for samples with a modulus in kPa to MPa scale while harder probes should be used for samples with a modulus in MPa scale and higher. The spring constant of a cantilever determines its sensibility and is mainly dependent on the cantilevers shape. Furthermore, the cantilevers material and shape determine the calculation model that is to be applied (see below). A probe with a small tip radius is suitable for soft samples and yields realistic results if the Sneddon theory is applied, while a probe with large tip radius is better for hard samples and application of a Hertzian model. Distance-Force curves can only be plotted if the deflection of the cantilever can be linked to the interaction force between tip and sample. This can easily be done by multiplying the deflection signal ΔU on the photodiode by the Deflection Sensitivity $\Delta\sigma$ and the s $pring\ constant\ k$ of the cantilever. The deflection sensitivity is the proportionality constant between the signal change at the photodiode [V] and the cantilever deflection [nm] and is given in [nm/V]. It is dependent on the laser position on the backside of the cantilever and must be recalibrated every time the spot position changes. For calibration purposes, the tip in indented on a very hard, rigid sample that does not deform. The Deflection Sensitivity can then be obtained

from the slope in the force-distance curve. The Thermal Tune method lately became the usual choice for determining the spring constant of the cantilever, as a result of its accuracy and lack of requirement for probe-sample contact[6]. In this method, the tip is far from the sample to avoid interactions, so the cantilever motion occurs only due to thermal fluctuations, which leads to a cantilever deflection of a few Å only (depending on the cantilever properties). The cantilever oscillation can be regarded as harmonically with one degree of freedom. According to the equipartition theorem, the force constant can be obtained by measuring the mean-square spring displacement according to equation [eq1].

$$k = \frac{k_B T}{\langle q^2 \rangle} \qquad ([eq1])$$

Where k_B is the Boltzmann constant, T is the temperature and q is the displacement of the oscillator (cantilever). The Power Spectral Density of the cantilever fluctuations is of Lorentzian shape. However, background noise contributes to these fluctuations. Practically, the Power Spectral Density of the cantilever thermal fluctuations are measured around its resonance frequency. Since background noise is not likely to have a resonance frequency in this area, it can easily be subtracted. The integral of the remaining peak is a measure of the power of the cantilever fluctuations and equals the mean square of the fluctuations $\langle q^2 \rangle$. The spring constant can thus be calculated using equation [eq2].

$$k = \frac{k_B T}{P} \qquad ([eq2])$$

where P is the integral of the power spectrum of the thermal fluctuations.

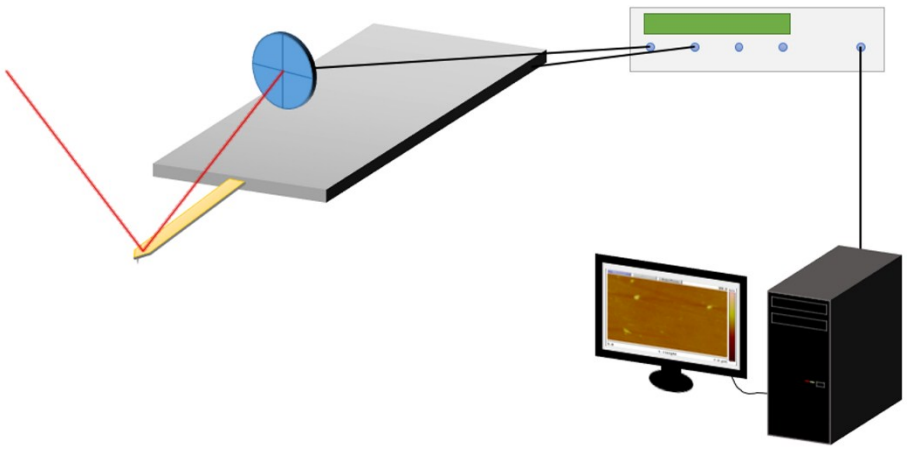

Figure S1. Basic Setup of an Atomic Force Microscope. A cantilever is placed onto a sample (latter is not shown here). The gold-coated backside of the cantilever reflects a laser beam onto a photodiode such that the latter can register any cantilever deflection as the tip scans the sample.

The change in signal of the photodiode is headed on to a controller that regulates the cantilever position and transfers the data to a computer.

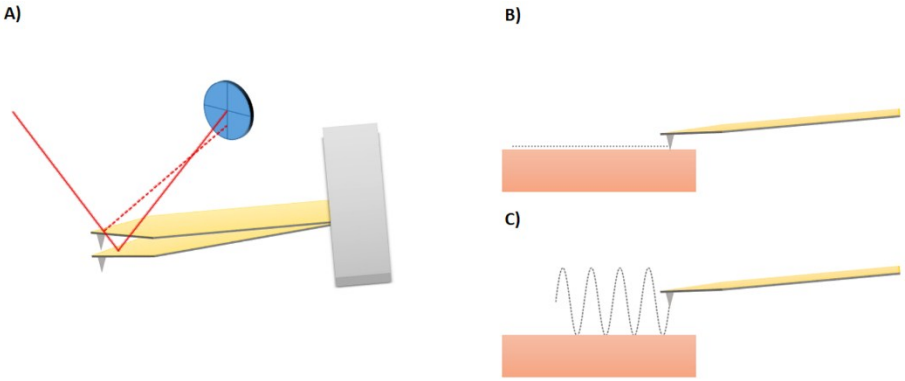

Figure S2. Deflection processing and measurement methods. A) A cantilever deflection results in a position change of the laser spot on the photodiode. B) In Contact Mode, the tip is in close contact to the sample. C) In TappingMode™ the tip oscillates above the sample, contacting it only slightly.

II) Different models of indentation evaluation methods

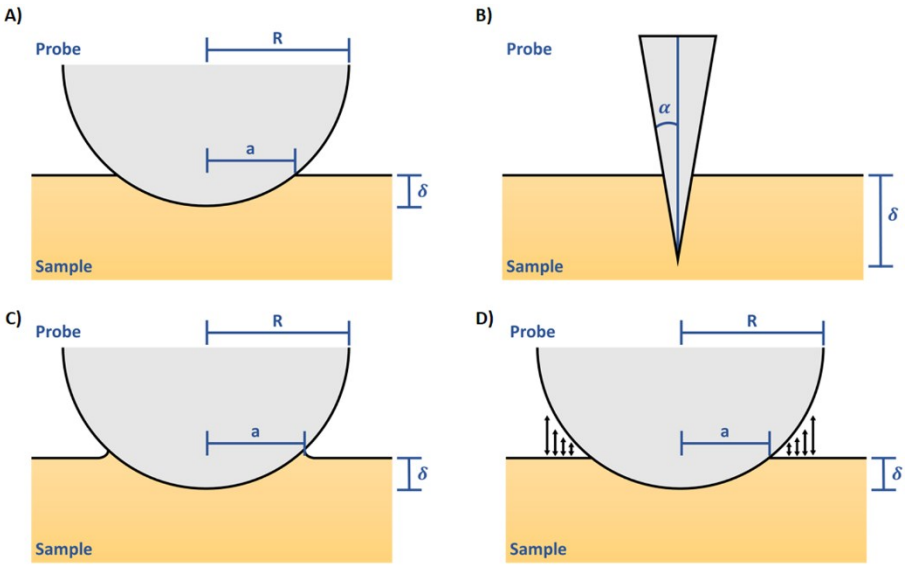

Figure S3. Comparison of indentation evaluation methods. A) With Hertz theory, a sphere indents a plane sample. Adhesion forces are neglected. B) The Sneddon method assumes a conical probe indenting plane. Again, adhesion forces are not taken into account. C) JKR Theory considers adhesion forces within the contact radius a. D) DMT model adds adhesion forces outside the contact area to the Hertzian model.

Elasticity transpired to be a principal factor on the nanoparticle uptake by cells. Several theoretic models are established to calculate elasticity from the indentation of a tip, each one exhibiting its specific advantages and disadvantages for specific probes and samples. In 1881, Heinrich Hertz was one of the first scientists to describe the contact mechanism between two bodies with curved surfaces and radii R_1 and R_2[7, 8]. He assumed that the two bodies could be described as two elastic half-spaces when $a \ll R_1$ and $a \ll R_2$, where a is the radius of the contact area of the bodies (see Figure S3 A). Assuming that there is no sheer stress, friction and adhesion between the two bodies, he could establish an equation for the pressure distribution from in the contact area.

$$p(r) = p_0 \cdot \sqrt{1 - \left(\frac{R}{a}\right)^2} \qquad \text{([eq3])}$$

with p_0 = maximum contact pressure. From this equation, he could derive an expression for the force F as a function of the penetration depth δ ([eq4]).

$$F = \frac{4}{3} E^* R^{\frac{1}{2}} d^{\frac{3}{2}} \qquad \text{([eq4])}$$

Where E^* is the effective elasticity and can be calculated using the Poisson ratios v_1, v_2 and elasticity moduli E_1 and E_2 with [eq5]. The effective radius R can be calculated similarly with [eq6].

$$\frac{1}{E^*} = \frac{1 - \nu_1^2}{E_1} + \frac{1 - \nu_2^2}{E_2} \qquad \text{([eq5])}$$

$$\frac{1}{R} = \frac{1}{R_1} + \frac{1}{R_2} \qquad \text{([eq6])}$$

Calculations using this model yield very accurate results if some requirements are met. Both the probe and the sample must consist of linear elastic, homogeneous and isotropic materials. In addition, the contact area between the two bodies must be minor compared to the dimensions of the bodies. Furthermore, other occurring forces like adhesion or friction are not considered. These demands are often met at macroscopic scale in the case of hard materials and yield realistic results in this area. However, the more a probe indents a sample, the more the ratio of a to R decreases, and thus with very soft samples, where the probe indents well past the very tip, the Hertzian model becomes inaccurate. In this case, the Sneddon model is regarded as a better approach. It yields a more generalized theory about the indentation of an axially symmetric probe into a sample when neither adhesion forces nor friction is taken into account. The general Sneddon equation is given in [eq7]

$$F = \frac{4Ga}{1-v}\int_0^1 \frac{x^2 \cdot f'(x)dx}{\sqrt{1-x^2}} \qquad ([eq7])$$

where G is the shear modulus of the probe, v is the Poisson number of the probe, $x = R/a$ and $f(x)$ is a geometrical function that describes the border strip of the probe. Using this equation with a spherical probe, the Hertzian model is obtained. Using it with a conical probe, [eq8] is obtained, when α is the angel between the main axis of the cone and its surface (see Figure S3 A).

$$F = \frac{2}{\pi} E^* \tan(\alpha) \cdot \delta^2 \qquad ([eq8])$$

This model yields satisfactory results when indenting a sharp probe to a soft sample. For accuracy, the probe tip radius should not exceed 10 nm and the indentation depth should be at least 30 nm. Both the Hertzian model and the Sneddon model allow an easy calculation of the elasticity from the increase of a force-distance curve (see Figure S4) using [eq4] and ([eq9]), respectively.

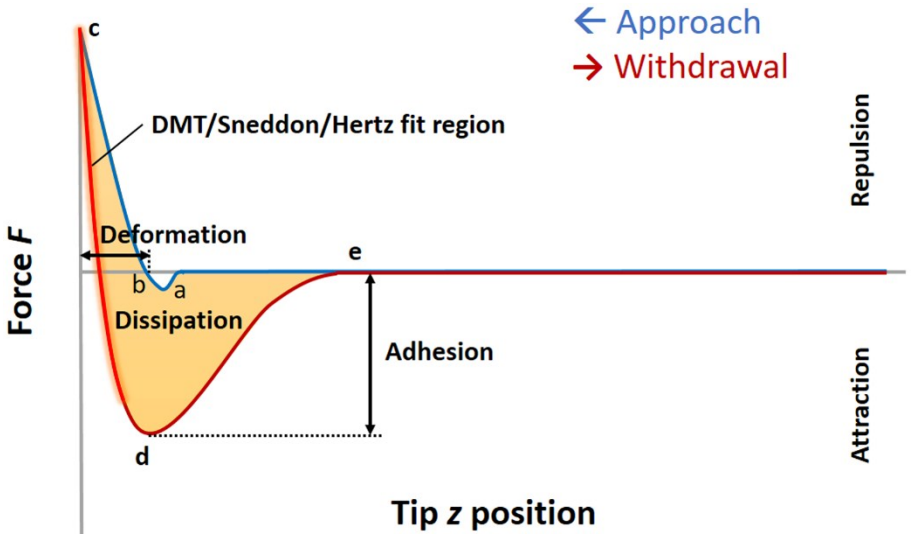

Figure S4. Typical Force-Distance Curve. As the tip approaches the sample (blue line, from right to left), the first interaction between tip and sample are attractive (a). As the tip further approaches repulsive forces predominate (b). At a certain point, the tip is withdrawn (c). Due to adhesion forces, the attractive forces at withdrawal are stronger than at approach (d). After contact breakdown tip deflection reaches zero again (e). Mechanical properties can be calculated as shown.

Nevertheless, for most probe-sample interactions at nanoscale, surface forces like adhesion and friction play a significant role and cannot be neglected. In 1971, Johnson, Kendall and Roberts

extended the theory of Hertz by considering the surface energy of the two approaching bodies (JKR-theory)[9]. If a spherical body is at short distance to a plane body, these bodies are attracted due to Van der Waals forces. Subsequently, the surface atoms are displaced, and a neck is built between the bodies (see Figure S3 C). This leads to a contact radius that is larger comparing to Hertz' theory.

The following equations are obtained by evaluating this model for the indentation depth δ, the contact radius a and the maximum adhesive force F_{ad}[10]:

$$\delta = \frac{a^2}{R} - \frac{4}{3}\sqrt{\frac{aF_{ad}}{RK}} \qquad \text{([eq9])}$$

$$a = \left[\frac{R}{K}\left(\sqrt{F_{ad}} + \sqrt{F + F_{ad}}\right)^2\right]^{\frac{1}{2}} \qquad \text{([eq10])}$$

$$F_{ad} = \frac{3}{2}\pi\gamma R \qquad \text{([eq11])}$$

Where γ is the work of adhesion per area, $K = \frac{4}{3}E\left(1 - \nu^2\right)$ is the elastic constant of the sample and F is the normal loading force. The JKR theory considers short distance adhesion forces within the contact area and elastic behaviour of the bodies. A specific characteristic of this model is the fact that when applying a tensile force after indentation the contact area is not decreased continuously. Instead the contact is lost at a critical force point $F_c < 0$. This critical force can be described in terms of the overall surface energy γ of the materials using [eq12].

$$F_c = -\frac{3}{2}\pi R\gamma \qquad \text{([eq12])}$$

Another model that is derived from Hertz' theory was established by Derjaguin, Muller and Toporov in 1975 (DMT theory)[11]. Just as JKR theory, the DMT theory takes adhesion effects between the two bodies into account. However, DMT theory assumes that within the contact area the stress profile remains Hertzian, i.e. no neck is built (see Figure S3 D). Instead, tensile stresses exist outside the contact area. This force must thus be added to the force obtained by the Hertzian model ([eq3]), hence resulting in [eq13].

$$F = \frac{4}{3}E^* R^{\frac{1}{2}}\delta^{\frac{3}{2}} + F_{ad} \qquad \text{([eq13])}$$

The adhesion force F_{ad} can easily be extracted from the force-distance-curve.

In summary, the JKR theory accounts for adhesion forces within the expanded area of contact only, while the DMT theory accounts for adhesion forces outside the contact area, only. The contradictions between these two theories could be clarified by Tabor in 1977[12-14], who showed that the JKR and the DMT theory were the extreme limits of one single theory described by the Tabor parameter μ which is defined as

$$\mu = \left[\frac{R(\Delta\gamma)^2}{E^{*2} z_0^3}\right]^{\frac{1}{3}} \qquad ([eq14])$$

Where z_0 is the equilibrium separation between the two surfaces in contact, $\Delta\gamma = \gamma_1 + \gamma_2 - \gamma_{12}$ is the work of adhesion, γ_1 and γ_2 are the surface energies of material of the spheres 1 and 2, respectively, and γ_{12} is the interfacial energy. The JKR theory applies for compliant solids with a large radius of curvature and large adhesion energy, hence $\mu > 5$, whereas the DMT theory applies for stiff solids with a small radius of curvature and small adhesion energy, hence $\mu < 0.1$.

A combined and upgraded elastic contact mechanism model was proposed by Maugis-Dugdale[15, 16]. Unfortunately, this solution is very analytical and requires experimental material data that are difficult to gather for unknown samples, which makes it difficult to be used for complementing AFM investigations. Table S1 gives an overview of benefits and limitations of the different models.

Table S1. Comparison of the various contact theory.

Theory	Assumptions	Limitations
Hertz	No surface forces, spherical probe, low loads only	Not valid for low loads if surface forces are present
Sneddon	No surface forces, conical probe (or probe with shape describable as function), deep indentation only	Not valid if surface forces are present
JKR	Short-ranged surface forces act only inside contact area	May underestimate loading due to surface forces
DMT	Long-ranged surface forces act only outside contact area	May underestimate contact area due to restricted geometry
Maugis-	Periphery of tip-sample interface modelled as a crack that fails at its	Analytical solution, but

III) Advanced peakforce QNM method

The usual way to assess the mechanical properties of nanomaterials is to measure their topography using Contact Mode or TappingMode™ and then to indent the tip at various locations selected by the user in the corresponding topographical image. This technique has several disadvantages. The acquisition of a high resolution topographical image can take a consistent amount of time, and only afterwards the force-distance curves can be recorded. In the meantime, single nanoparticles may have experienced a small displacement which can lead to an incorrect positioning of the probe when nanoparticle intendation is desired (e.g. next to the nanoparticle or at its very edge instead of its centre). Furthermore, this technique is very time-consuming since every single force-distance curve must be evaluated individually. It hence does not really allow a full mapping of the measured sample area.

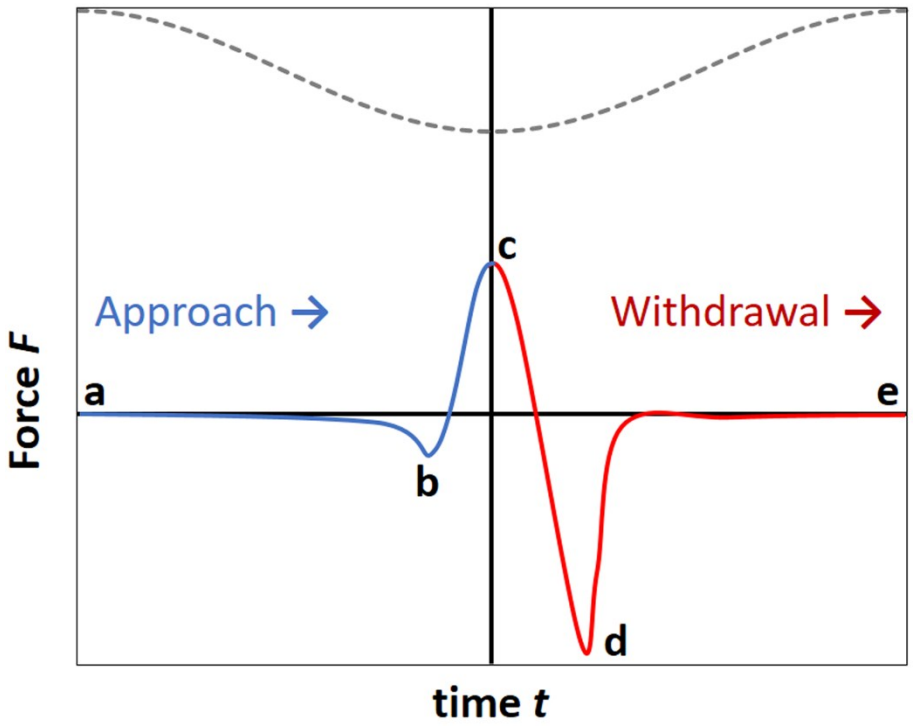

Figure S5. Single PeakForce Tapping indenting[17]. The grey dashed line at the top shows the *z* position of the piezo, while the blue and red lines show the cantilever deflection due to tip-sample interaction. At the beginning, there is no interaction between tip and sample (a). Approaching, the first interaction will be attractive (b), before repulsive interactions dominate (b). At a definite point (PeakForce, (c)), the indenting stops and the tip is withdrawn. Adhesion forces lead to a

deflection (d) until the tip snaps off the sample and there is no more interaction forces (e). cf. Figure S4.

As described above, TappingMode™ was a huge improvement to visualise a sample topography without damaging neither tip nor sample, since they are in contact for a very short time per tip movement circle only. Peak Force Tapping Mode (2009) is an enhanced technique to measure the topography of a sample area at high resolution while yielding the mechanical properties of every single point of this sample area, so as to gain a full mechanical sample mapping[5, 17, 18]. To do so, the Tapping Mode is extended by a modulation frequency of about 1 to 2 kHz when the tip gets in contact with the sample surface. Unlike TappingMode™, the maximum force on the tip (*Peak Force*) is controlled and not extended upon a certain value. Figure S5 shows the z Piezo of the probe (dashed line) and the deflection of the cantilever (blue and red line), both plotted versus time. At point a, the tip is not in contact with the sample surface yet. At point b, a so-called *Snap-On* occurs, when the tip is attracted to the sample surface due to van der Waals, electrostatic or capillary forces. As the probe further approaches the sample surface, repulsive forces predominate. When the peak force is reached (point c), the tip is withdrawn from the surface. As mentioned above, tip and sample stay in contact due to adhesive forces until the critical force is reached (point d). After that, there is no more measurable interaction between tip and sample (point *e*) and the sinoidal swinging takes the cantilever to the next point that is to be analysed. The whole procedure from point *A* to point *E* takes about 0.5 ms. For better evaluation the recorded force is plotted versus the tip-sample separation to obtain a force-distance curve (see Figure S4). From this curve, mechanical properties including elasticity, adhesion, dissipation and others are directly calculated and mapped.

This technique not only saves a lot of time, but is also more accurate since topographical imaging and nanomechanical mapping happen simultaneously. Another advantage is the soft interaction between sample and probe since every point is stressed to the peak force only, which prevents damage.

IV) References

1 K. C. Neuman and A. Nagy, *Nat. Methods*, 2008, **5**, 491-505.
2 G. Binnig, C. F. Quate and C. Gerber, *Phys. Rev. Lett.*, 1986, **56**, 930-933.
3 N. A. Burnham and R. J. Colton, *J. Vac. Sci. Technol. A*, 1989, **7**, 2906-2913.
4 B. Cappella and G. Dietler, *Surf.Sci. Rep.*, 1999, **34**, 1-+.
5 J. L. Hutter and J. Bechhoefer, *Rev. Sci. Instrum.*, 1993, **64**, 3342-3342.
6 H. Hertz, *J. Reine Angew. Math.,* 2009, **1882**, 156-171.
7 V. L. Popov, Rigorose Behandlung des Kontaktproblems – Hertzscher Kontakt, 2010.
8 I. N. Sneddon, *Int. J. Eng. Sci.*, 1965, **3**, 47-57.
9 Y. M. Efremov, D. V. Bagrov, M. P. Kirpichnikov and K. V. Shaitan, *Colloid. Surface. B*, 2015, **134**, 131-139.
10 B. V. Derjaguin, V. M. Muller and Y. P. Toporov, *Prog. Surf. Sci.*, 1994, **45**, 131-143.
11 D. Tabor, *J. Colloid. Interf. Sci.*, 1977, **58**, 2-13.
12 V. M. Muller, V. S. Yushchenko and B. V. Derjaguin, *J. Colloid. Interf. Sci.*, 1980, **77**, 91-101.

13 M. Ciavarella, J. A. Greenwood and J. R. Barber, *J. Mech. Phys. Solids*, 2017, **98**, 236-244.
14 D. Maugis, *J. Colloid. Interf. Sci.*, 1992, **150**, 243-269.
15 D. Maugis, *Contact, Adhesion and Rupture of Elastic Solids*, Springer Berlin Heidelberg, 2000.
16 X. H. Shi and Y. P. Zhao, *J. Adhes. Sci. Technol.*, 2004, **18**, 55-68.
17 B. Pittenger, N. Erina and C. Su, *Solid. Mechanics & Its Applications*, 2014, **203**, 31-51.
18 K. L. Johnson, K. Kendall and A. D. Roberts, *Proc. R. Soc. Lond.*, 1971, **324**, 301-313.